Proceedings of the
Annual Stability Conference
Structural Stability Research Council
Baltimore, Maryland, April 10-13, 2018

Geometric Imperfections in Shell Finite Element Models of CFS Members - A Review of Current State of Practice

Shafee Farzanian[1], Arghavan Louhghalam[2], Benjamin W. Schafer[3], Mazdak Tootkaboni[4]

Abstract

In cold-formed steel structures (CFS), the ultimate strength, stiffness, and post-buckling behavior are highly susceptible to geometric nonlinearity, in addition to material yielding or nonlinearity. It has long been standard practice in research to include initial geometric imperfections in shell finite element collapse simulations. The purpose of this paper is to provide a summary of efforts geared towards characterizing and modeling geometric imperfections in their full three-dimensional spatially varying forms. A close look at different geometric imperfection models proposed in the literature, reveals that, while seemingly different, almost all of these models express an imperfection profile by three components: imperfection shape, magnitude, and combination coefficient. Herein, the details required to setup high fidelity shell finite element nonlinear collapse analysis of CFS members to mimic the multitude of different imperfection models are presented. A careful comparison of the different strategies in seeding geometric imperfections shows a noticeable variability in the load carrying capacity and the stability behavior. The insights drawn from this work support our overall goals of developing an advanced analysis-based design framework for CFS members, through applying data-driven stochastic modeling, and providing a platform for the validation of code-prescribed or practice-oriented geometric imperfection models.

1. Introduction

Cold Formed Steel (CFS) members belong to a unique class of structures, thin-walled structures where pushing the efficiency in performance and cost to its boundaries is achieved through extreme material minimization. This often leads to ultra-thin or ultra-slender structures that undergo sudden large deformation under loading, known as mechanical instabilities or buckling. CFS structural members are made by rolling or pressing thin sheets of steel into a variety of shapes at room temperature. These structures like any other fabricated structure possess imperfections that are a result of manufacturing, shipping, storage, and construction processes. These imperfections, often random in nature, are either in the form of the difference between the actual or physical values and the nominal values for material properties such as modulus of elasticity, yield stress, and residual stresses and strains (material imperfections) or Geometric Imperfections (GI) that pertain to

[1] Research Associate, University of Massachusetts Dartmouth, <shafee.farzanian@umassd.edu>
[2] Assistant Professor, University of Massachusetts Dartmouth, <alouhghalam@umassd.edu >
[3] Professor, Johns Hopkins University, <schafer@jhu.edu >
[4] Associate Professor, University of Massachusetts Dartmouth, <mtootkaboni@umassd.edu >

deviation of the member from perfect geometry. The Load Carrying Capacity (LCC) of CFS members like any other thin-walled structure is highly influenced by geometric nonlinearity. Therefore, initial GIs play a key role in ultimate strength, stiffness, and post-buckling behavior of CFS members. As a result, close replication of mechanical response observed in experiments, requires advanced measuring techniques for accurate characterization of GI, and use of proper simulation procedures. A close look at different GI models proposed in literature (see Section 2), reveals that, while seemingly different, almost all of these models assume an imperfection profile in the following form:

$$G(x,y,z) = \sum_{i=1}^{n} c_i \alpha_i \, \varphi_i(x,y,z) \tag{1}$$

where, ϕ_i is the imperfection shape, α_i is the magnitude, and c_i is a combination coefficient. This imperfection form is inspired by the fact that such members are sensitive to geometric imperfection shapes that are affine to the member eigenbuckling mode. The ϕ_i in the preceding expression are often inherent attributes of CFS members and depend on several factors including section profile, member length, loading condition, etc. They are either simple trigonometric functions representing individual plate buckling modes, or the critical mode shapes of the whole member, or are selected to be the critical mode shapes spanning certain classes of deformation such as cross-sectional and global deformations. Imperfection mode shapes are usually obtained via Finite Element (FE) analysis and/or semi-analytical techniques such as Finite Strip Method (FSM). Global imperfection mode shapes, however, can be approximated well by rigid body translation or rotation of cross-section in the form of single half-sine wave along the member. The α_i values can be obtained from statistics of measured imperfections, from simple empirical relations, or based on quality control tolerances (see Section 2). The c_i values, on the other hand, pertain to how to combine the imperfections to find the lowest LCC, or the LCC that is close to experimental observations, and are obtained in such a way that a suitable norm of the coefficient vector equals to 1:

$$\|c\|_2 = \sqrt{\sum_{i=1}^{n} c_i^2} = 1 \tag{2a}$$

$$\|c\|_\infty = \max(|c_i|) = 1 \tag{2b}$$

For simplicity, researchers have classified the general forms of GI in Eq. 1 into five modal imperfections; i.e., the so-called traditional modal approach. The global or overall out-of-straightness is a deviation of whole member from straightness, or the rigid body translation or rotation of the cross-section from its perfect position. The cross-sectional imperfection is a form of inaccurate section dimensions or general waviness in the section shape where cross-sectional elements distort individually. Global imperfections are either divided into bow, camber, and twist modes reflecting sweeps about the weak, strong, and longitudinal axes of the member (passing through the shear center), respectively or any combination thereof. Cross-sectional imperfections are divided into local and distortional with the former corresponding to plate (web or flange) buckling at specific locations and the latter pertaining to the rotation of the flange at the web/flange junction or the displacement of stiffener element (lip) normal to its plane. Within a distortional mode, cross-sectional elements buckle together with a relatively longer wave length than that of local mode.

This paper aims at providing a brief summary of efforts aimed at characterizing and modeling GI in CFS members. The FE implementation details for nonlinear collapse analysis of imperfect CFS structural members are laid out. A comparative study of numerical results obtained with different GI modeling strategies is provided. The presented results are part of an ongoing comprehensive study (Farzanian et al. 2018a, Farzanian et al. 2018b) that is focused on developing a probabilistic framework for the validation of code-prescribed or practice-oriented geometric imperfection models.

2. Review of geometric imperfection modeling

The literature on nonlinear collapse analysis of CFS members is ripe with many GI models that have been proposed by researchers and different structural design codes. In what follows, we review some of these models that relate directly to the discussion in the preceding section on imperfection shapes $\varphi_i(x, y, z)$, magnitudes α_i, and combination coefficients c_i with the goal of informing nonlinear FE modeling procedures that aim at characterizing the load carrying capacity of CFS members (Farzanian et al. 2018a).

2.1 Dawson and Walker (1972)

Dawson and Walker (1972) presented closed form solutions for elastic local buckling of simply supported plates with stress free edges considering the geometric imperfections. The behavior of such plates is similar to individual assembly elements of thin-walled members. Explicit expressions for LCC, end shortening, and stiffness of these members were derived and the shape of initial geometric imperfection was assumed to be the same as plate buckling mode:

$$w_0 = t \sum_{i=1,3,\dots}^{\infty} \sum_{j=1,3,\dots}^{\infty} a_{ij} \cos\frac{i\pi x}{a} \cos\frac{j\pi y}{b} \tag{3}$$

where a, b, and t are length, width, and thickness of plate, respectively and a_{ij} are prescribed coefficients such that

$$e_0 = \sum_{i=1,3,\dots}^{\infty} \sum_{j=1,3,\dots}^{\infty} a_{ij} \tag{4}$$

is the amplitude of the initial geometric imperfection at $x = 0$ and $y = 0$. Dawson and Walker considered three different expressions proposed by other researchers (Winter 1947, Dutheil 1952, Chilver 1953) to estimate the magnitude of the local imperfections:

$$e_0 = \alpha \tag{5a}$$

$$e_0 = \beta\left(\sigma_y/\sigma_{cr}\right)^{0.5} \tag{5b}$$

$$e_0 = \gamma\left(\sigma_y/\sigma_{cr}\right) \tag{5c}$$

where α, β, γ are general constants to be determined experimentally, σ_y is the yield stress, and σ_{cr} is the critical buckling stress of CFS members. Although, assuming $\alpha = \beta = \gamma = 0.2$ in the above equations provided adequately conservative results, they recommended Eq. 5c with $\gamma = 0.2$ as the most suitable generalized imperfection amplitude for the analysis of CFS members.

2.2 Chou and Chai (1997)

Chou and Chai (1997) performed post-buckling FE analysis of thin-walled structural members to propose a design procedure. The LCC of a set of stub-columns with geometric imperfections was numerically determined. To validate the results, a comparison with experimental data and BS 5950 (1987) was performed. The geometric imperfection shape was inspired by buckling mode shapes obtained from eigenvalue analysis. Two cases were modeled; small perturbation forces applied at a single plane at the middle of member, and perturbation forces at multiple (four) planes at the extrema of the first mode shape along the member. The former leads to a half sine wave which is typically the first buckling mode for long columns. Also, the values of such transverse forces were first estimated for a benchmark specimen and then calculated for other stubs invoking empirical expressions. Three sets of force values with a constant ratio were chosen to represent different degrees of initial imperfection. One issue with this approach is that the benchmark force values are calibrated with given experiments and force amplitudes for other stub-columns depend on the ratio of cross-sectional areas for the stub-column under investigation and the benchmark stub-column. This results in the same degree of imperfection for the two specimens with same cross-sectional area and different thicknesses which is counter intuitive since a thinner section typically has a higher potential for imperfection. Through comparison with experiments and BS 5950 code, they showed that FEA results were consistently conservative. Therefore, they proposed a constant correction factor for predicting the ultimate load in their design procedure.

2.3 Schafer and Pekoz (1998)

Schafer and Pekoz (1998) suggested two approaches for geometric imperfection modeling that consider both imperfection shape and magnitude. To perform a limited study, they suggested that at least two fundamentally different eigenmode shapes be summed together for the imperfection shape. Such modes should not be the same fundamental modes with a different wavelength. It was shown as an example that seeding a GI pattern with only local or only distortional eigenmode is conservative when compared to seeding both modes which implies the importance of properly combining eigenmodes to form the GI pattern. As for the magnitude, Schafer and Pekoz proposed the maximum values for local and distortional GI using empirical expressions (simple rules of thumb) and probabilistic analysis (Table 1). In empirical relations, two values at representative points were introduced; d_1, the maximum local GI at the middle of the web in the form of out-of-flatness of the web plate, and d_2, the maximum deviation at flange-lip intersection or its out-of-straightness for distortional GI. Based on collected data, it was suggested that local imperfection be in the form of either Eq. 6a (in terms of plate width w) or Eq. 6b (in terms of plate thickness t) assuming $w/t < 200$:

$$d_1 \approx 0.006w \tag{6a}$$

$$d_1 \approx 6te^{-2t} \quad (d_1 \; and \; t \; in \; mm) \tag{6b}$$

A similar expression for distortional imperfection magnitude (valid for $\mathrm{w/t} < 100$) was proposed:

$$d_2 \approx t \tag{7}$$

where the thickness should be less than 3 mm for both Eq. 6 and 7 to be valid. Noticing a large variation in measured maxima, Schafer and Pekoz recommended more conservative maximum magnitudes. They presented the cumulative distribution function (CDF) values of d_1/t and d_2/t for the measured data (see Table 1) which are in good agreement with additional measurements. These percentile values enabled the connection between confidence level and a particular imperfection magnitude. To perform a more comprehensive study, they proposed the use of imperfection spectrum of the GI signal (along the member); See (Farzanian et al. 2018b) for further details.

Table 1. CDF values for maximum imperfection (Schafer and Pekoz 1998)

	Type 1	Type 2
$P(\Delta < d)$	d_1/t	d_2/t
0.25	0.14	0.64
0.50	0.34	0.94
0.75	0.66	1.55
0.95	1.35	3.44
0.95	3.87	4.47
Mean	0.50	1.29
St. dev.	0.66	1.07

2.4 Sivakumaran and Abdel-Rahman (1998)

Sivakumaran and Abdel-Rahman (1998) proposed GI patterns and magnitudes for specific CFS members and validated FE results through a test program. A set of perforated and non-perforated lipped channel stub-columns with different lengths under axial compression was examined. The columns were short enough to eliminate the global buckling mode but long enough to accommodate various size of perforations as well as to allow longitudinal propagation of local buckling mode. The length of non-perforated columns was selected to be $3\left(w + w_f\right)/2$ with w the web width and w_f flange width. The length of perforated columns was then increased in proportion to the size of perforation.

Inspired by local buckling shape of an individual plate and modifying Hancock's (1979) suggestion for distribution of plate imperfection in CFS columns, they seeded the GI profile only within the web (and not within the flange or the lip) as a double sine-wave distribution:

$$\delta = \delta_0 \sin\left(\frac{\pi x}{w}\right) \sin\left(\frac{\pi y}{\overline{w}}\right) \tag{8}$$

with $\overline{w}$ the average of the web and flange widths. So, the GI pattern is one half-sine wave in transverse direction of web and multiple half-sine waves with a wave length of $\overline{w}$ in its longitudinal direction. Also, δ_0, which is the imperfection magnitude at the central point of the web plate which was selected to be one-half of the upper limit recommended by BS 5950, i.e.

$$\frac{\delta_0}{t} = 0.5 * 0.145 \left(\frac{w}{t}\right) \sqrt{\frac{F_y}{E}} \tag{9}$$

where t is thickness, w/t is slenderness ratio, and E and F_y are material properties of plate.

2.5 Sun and Butterworth (1998)

Sun and Butterworth (1998) conducted FE analysis on steel single angle members under compression and eccentric loading applied to one leg. The nonlinear stress-strain curve with an elastic part, a perfectly plastic part, and a multilinear strain hardening, based on test data was used. For the initial GI pattern, they adopted several half-sine waves in the longitudinal direction and linear variation in the transverse direction resembling a typical local buckling mode. It should be mentioned that such GI shape implies the first buckling mode of this certain steel member. They used initial imperfection amplitudes of $0.167t, 0.333t, 0.5t$, and $0.667\mathrm{t}$ in their analyses. The results were then compared with experimental tests to calibrate the amplitude for the prediction of LCC and buckling behavior. Equal leg struts (EA 90x90x6) with four lengths were chosen for tests. The high width/thickness ratio of the section gave rise to local buckling and the varying slenderness ratios from 50 to 150 lead to both elastic and inelastic buckling behavior. It turned out that the $0.333t$ amplitude was the best match for ultimate loads although the post buckling behavior was not predicted properly. Also, the effect of two different directions c_i (twisted first half-sine wave about the shear center in (anti)clockwise direction) of initial wave was investigated. Except for the most slender member, the impact was tangible for both load carrying capacity and post-buckling behavior. Finally, a parametric study on 200+ (un)equal leg struts was performed to compare the results with the nominal loads prescribed by NZS 3404 (1997) for a wide range of slenderness ratios (30 to 300) and scaling factors were proposed to adjust the values recommended by NZS 3404 (1997).

2.6 Chou et. al. (2000)

Chou et. al. (2000) examined the post-buckling behavior of cold formed lipped channel and hat-section stub-columns under axial compression. They compared the numerical results with experimental data by Zaras and Rhodes (1987) as well as BS 5950 predictions. For initial GI pattern they used exact linear buckling modes in contrast to their previous work (Chou and Chai 1997) where they used small perturbation loads. For α_i values, they used $0.10t, 0.50t, 1.00t$ and Walker's (1969) expression for imperfection magnitude, $0.3\left(P_y/P_{cr}\right)^{0.5}t$, where t is member thickness, P_y yield load, and P_{cr} critical buckling load. They applied two safety factors (1.25 and 1.18) in their proposed design procedure to reduce all overestimated numerical results to values bellow the test results.

2.7 Gardner (2002)

Gardner (2002) performed experiments and numerical simulations on cold-formed stainless steel members and compared the results with the predictions of Eurocode (EC 3: Part 1.4) to propose a consistent approach for the modeling of stainless steel structures. The investigated members comprised Square, Rectangular, and Circular Hollow Sections (SHS, RHS, and CHS respectively) under variety of loading and boundary conditions including stub-columns (37 specimens), pin-ended columns (22 specimens), and simply-supported beams (9 specimens). Proper material modeling assumptions including appropriate stress-strain behaviors and residual stresses were considered in the FE simulations to enable better replication of test results.

To seed the initial GI, the eigenmodes obtained from elastic buckling analysis were used. For stub-columns with SHS, RHS, and CHS sections, only the local buckling mode shape (the lowest buckling mode) was used. The short stub-columns $(180\ mm\ \leq L \leq 450\ mm)$ failed by local buckling, a failure mode that was in agreement with test experiments. However, for pin-ended columns (with SHS and RHS sections) that typically buckle into global mode shape, the superposition of both global and local modes obtained from the first few eigenmodes was proposed as the GI pattern. As for the seeding of GI in beam specimens, the lowest eigenmode in pure compression (similar to those selected for the corresponding stub-columns) was used; The in-plane bending failure mode for all beams was in the form of local buckling of the compression flange and the top portion of the web.

For imperfection amplitude, the measured values of local and global imperfections as well as empirical relations (Eq. 5 for cold-formed carbon steel members) were used in FE simulations and their results were compared with experimental tests. The linear regression analysis on measured local imperfection amplitudes for SHS and RHS stainless steel members showed the best fit for $\beta = 7.3 * 10^{-6}$ and $\gamma = 0.023$ in Eq. 5b and 5c, respectively. The results obtained from numerical simulations with imperfection amplitudes defined by Eq. 10 demonstrated accurate agreement with test results and therefore Eqs. 10 and 11 were suggested for local imperfection amplitude of SHS and RHS members, and CHS members:

$$\omega_0/t = 0.023(\sigma_{0.2}/\sigma_{cr}) \tag{10}$$

$$\omega_0/t = 0.2 \tag{11}$$

where $\sigma_{0.2}$ is the material 0.2% proof stress, ω_0 is the imperfection amplitude, and t is the thickness. For beam specimens, the local imperfection amplitude was selected similar to those of stub columns. Based on the parametric study and comparison with test results for SHS and RHS pin-ended columns, Eq. 12 for global imperfection amplitude was proposed:

$$v_0/L = 1/2000 \tag{12}$$

where v_0 is the global imperfection amplitude in buckling direction and L is the specimen length.

2.8 Zeinoddini (2011)

Zeinoddini (2011) adapted different approaches for GI modeling and nonlinear collapse analysis to examine failure mechanisms for CFS members. Different bracing configurations were used to invoke such failure modes as local, distortional, and felxural torsional for a 362S162-68 profile (SSMA 2011 nomenclature) of length $2.44\ m$. As-measured imperfections were seeded in the form of perturbations in the perfect geometry and mechanical interpolation was used to extend the measured imperfections to the points with no measurement. In mentioned work, the data reported by Peterman and Schafer (2014) was applied to the member as displacement loading. A combination of the buckling mode shapes corresponding to the lowest eigenvalues (the traditional modal approach) was also used to seed geometric imperfections. The mode shapes were obtained via CUFSM (Schafer and Ádány 2006) and were used as local, distortional, and (mixed) global imperfections with the latter encapsulating bow, camber, and twist imperfections which can be seeded separately as half-sine waves as well. Several ($3^3 = 27$) combinations for c_i equal to $(-1, 0, +1)$ with $c_i = 1$ ($c_i = -1$) representing the existence of a mode with positive (negative) sign and $c_i = 0$ representing the absence of a mode, and all α_i values equal to $50\%ile$ of all measured data (Table 6-1 in (Zeinoddini-Meimand 2011)) were considered. Both 25% and 75% imperfection exceedance values with $c_i = 1$ were also examined to explore the effect of magnitude on response. More sophisticated approaches for simulating imperfections (e.g., spectral representation) were also used by Zeinoddini and Schafer (2012).

3. Nonlinear shell buckling analysis: model setup and implementation details

Owing to the complexity of nonlinear stability behavior of CFS members, numerical solution techniques such as FEM are often used to study their load carrying capacity and post-buckling response. This section describes the details required to setup FE models for nonlinear collapse analysis of CFS members using the general purpose commercial software package, ABAQUS, including the analysis types, material properties, element type and size, loading and Boundary Conditions (BCs), and most importantly the seeding of GI onto the perfect model. To facilitate the creation of input models, an in-house Python script (Farzanian and Shahsavari 2018) coupled with CUFSM software is employed to automate the repetitive tasks pertaining to model setup and implementation details, including those related to generating a multitude of GI models. Fig.1 depicts a schematic of a 3D computational model (a lipped channel CFS member) with exaggerated magnitudes of GI encompassing five classified modal imperfections.

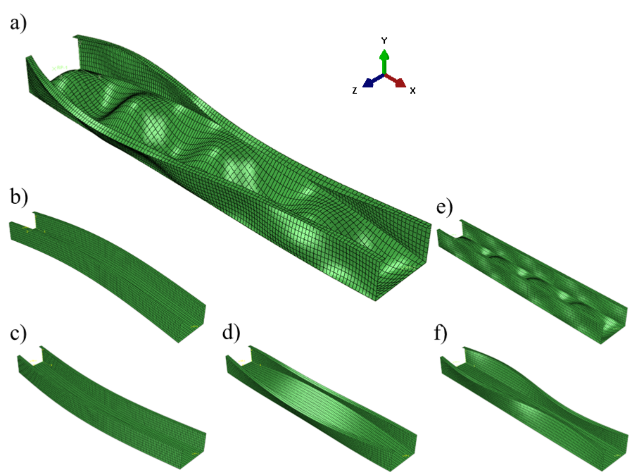

Figure 1: Computational model with GI as (a) combination of 5 classified modes including: (b) bow (c) camber (d) twist (e) local (f) distortional

3.1 Analysis types

When it comes to shell stability analysis, commercial FE software packages such as ABAQUS offer a variety of analysis options. The linear-buckling analysis (also called eigenvalue buckling analysis, or bifurcation buckling analysis) is the most common and predicts the theoretical buckling strength (elastic buckling strength) which is of great importance specially for stiff structures with almost linear prebuckling response. Although the nonlinear behavior and post buckling response cannot be captured by eigenvalue analysis, the buckling modes extracted from a bifurcation buckling analysis are typically used to inform the shape of geometric imperfections that are seeded into the perfect model for nonlinear analysis. Open source software packages based on semi-analytical techniques such as CUFSM are also an attractive alternative for eigenvalue buckling analysis as they provide a means to classify the buckling mode shapes to cross-sectional (local and distortional) and global modes. In a fully nonlinear collapse analysis aimed at estimating LCC and capturing the post-buckling behavior, however, concerns such as material nonlinearity, geometric nonlinearity prior to buckling, or unstable post-buckling response need to be addressed. Several approaches in ABAQUS allow for modeling the complex behavior in post-buckling regime where the load-displacement response shows a negative stiffness and the structure releases strain energy to remain in equilibrium. One alternative is to make recourse to dynamic analysis taking into account the inertia effects as the structure snaps. Another approach is to use artificial damping to stabilize the structure during a static analysis. ABAQUS offers an automated version of this stabilization approach for the static analysis procedures which is the one used for this study. Alternatively, static equilibrium path during the unstable phase of the response can be traced by using the modified Riks method (Crisfield 1981). The Riks method works well in snap-through problems (e.g., post-buckling problems with unstable behavior), those in which the equilibrium path in load-displacement space is smooth and does not branching (bifurcating). However, the exact post-buckling problem cannot be analyzed directly due to the discontinuous response at the point of buckling. To this end, it must be turned into a model with continuous response instead of bifurcation which is already satisfied for analyses of our imperfect models. Thus, to control the onset of buckling, special precautions need to take for choosing the magnitude of imperfections; in particular, for structures that show linear behavior prior to (bifurcation) buckling. Otherwise, in the absence of GI, buckling will be initiated by by discretization errors.

3.2 Material properties

Accurate modeling of the basic material properties is of crucial importance if the modeling of CFS member is to resemble the behavior observed in the lab. Although, the focus of this study is to provide a comprehensive review of GI modeling and its interplay with LCC, realistic material based on coupon tests performed at Johns Hopkins University Thin-Walled Structures Group (Vieira Jr and Schafer 2012) are used in all FE simulations; the stress-strain curve adopted from (Zeinoddini-Meimand 2011) is used and the Poisson's ratio is assumed to be 0.30.

3.3 Element type and size

CFS members are usually modeled with shell elements as through-thickness deformation and tri-axial stresses are not expected to be significant. ABAQUS offers a wide variety of elements for shell modeling (e.g., S4, S4R, S4R5, S8R, etc.). Element type S9R5 is used in our study. Different mesh densities were examined to achieve convergence. The convergence study and the seeding of GI models were facilitated with our in-house Python code. Finally, to avoid element distortion in large deformations, the aspect ratio of elements is kept between 0.5 and 2 and orthogonal meshing aligned with the orientation of member's longitudinal axis is used.

3.4 Loading and boundary conditions

As mentioned in Section 3.1 to seed certain classes of GI, the imperfection shapes are borrowed from buckling modes of the perfect member which implies that the Boundary Conditions (BCs) in FE model used for nonlinear analysis and the model used for buckling analysis need to match. This issue needs to be addressed carefully in cases where a numerical technique other than FEM is used for buckling analysis. For example in FSM, the semi-analytical technique that is the basis of CUFSM, the end constraints are enforced by adopting particular shape functions in the longitudinal direction that meet the end conditions a priori. Further details for the equivalent FE BCs matching FSM BCs, can be found in (Ahmadi et al. 2018).

3.5. Initial geometric imperfection

To seed a particular GI into a computational model, three ingredients forming Eq. 1 need to be determined; i.e., imperfection shape, magnitude, and combination coefficient (see Section 2). We note, however, that regardless of the approach adopted, the imperfect member is always assumed stress-free at the onset of analysis. A common approach to choose the shape of GI is to use simple spatial variations resembling individual plate buckling modes. Our in-house Python code adjusts the positions of the individual nodes in FE models to replicate the known mode shape. Another approach is to use the lowest mode shapes for the whole member which can be directly obtained from a linear buckling analysis using, say, ABAQUS. Such eigenmodes are multiplied by a scaling factor (imperfection magnitude α_i) before they are superimposed to the perfect model. The third approach is perturbing the perfect model with certain classes of imperfections including cross-sectional and global imperfections which can be obtained from elastic buckling analysis using a semi-analytical software, say CUFSM, which has the ability to categorize and reduce the complicated deformations through projecting them onto a set of basis forms. This approach, on one hand allows for direct application of buckling modes as GI patterns and on the other hand makes it easier to connect the magnitude of GI to measured data. This is of particular importance, considering the fact that geometric imperfections are a result of fabrication and other processes. In fact, to inform an analysis-based design framework that relies on the data from the field, the approach adopted for GI modeling should allow the seeding of a wider set of geometric imperfections beyond the oversimplified models in first approach or the fundamental (or lowest) eigenmodes in second approach. In other words, for a specific CFS member, the lowest eigenmodes obtained from FE analysis may or may not contain a particular mode which is further explained in Section 4.

In addition to aforementioned GI models, the nodal coordinates of imperfect CFS members can be obtained from measuring the geometry of real samples directly. To identify these coordinates in FE modeling, appropriate data processing and geometric transformations--that depend on the measurement platform; see (Zeinoddini-Meimand 2011, Peterman 2012, Zhao et al. 2015, Zhao et al. 2017)--are required. The LCC results of proposed GI models can then be compared with those of the FE models with as-measured imperfections. Such measured imperfections can also be used to develop data-driven stochastic framework and validation metrics for careful examination of geometric imperfections (Farzanian et al. 2018b).

4. Classic modes

The first buckling mode of a whole CFS member depends on both its cross-section and length. Herein, we characterize three representative CFS lipped channel sections with different expected dominant buckling modes (see Fig. 2) using FSM and cFSM (Li and Schafer 2010) stability solutions in order to provide arbitrary classified modal imperfections for any CFS member. The Simple-Simple BC is adopted for all cases.

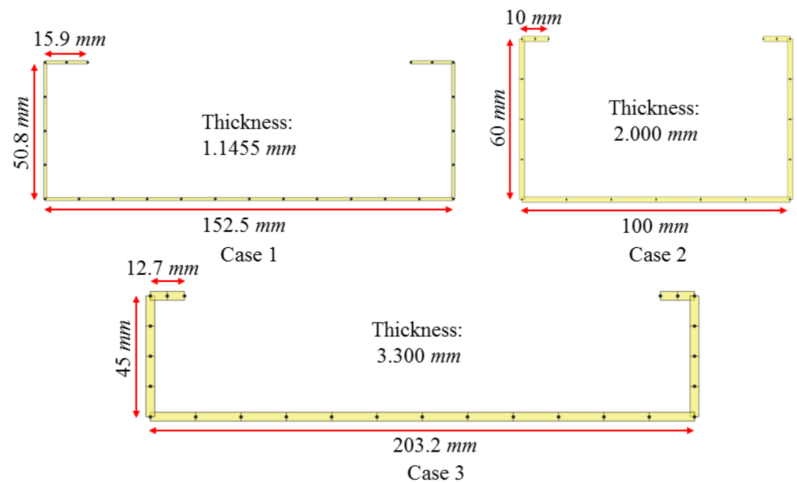

Figure 2: Geometry of three CFS lipped channels cross-sections (a) Case 1 (b) Case 2 (c) Case 3

Fig. 3 represents the conventional FSM stability solutions augmented with pure mode cFSM solutions for three cases (panels a-c in Figure 3 correspond to cases 1-3 in Figure 2). Each panel contains the signature curve ($m = 1$ only, in red), the single term stability solutions up to $m = 15$ (in green), and the so called "many-term" solution comprising all 15 terms (black dashed line), all obtained using CUFSM. The signature curves (red) often provide the necessary information for the local, distortional, and global buckling modes assuming one half-sine wave along the member. For example, in Fig. 3a, the two local minima at half-wavelengths of 116 and $570\ mm$ correspond to critical local and distortional buckling modes, respectively, and the descending branch at longer lengths ($\sim L > 1500\ mm$) corresponds to global mode. The same values for Case 2 (Fig. 3b) are 84 and $353\ mm$ and the lengths higher than $\sim 750\ mm$. However, for particular cross-sections, similar to Case 3 in Fig. 3c, the signature curve may fail to identify the buckling modes. In such cases, to warrant the extraction of pure buckling mode shapes for the aim of imperfection seeding, constraint FSM (cFSM) analysis can be used. The pure local (blue), distortional (black), and global (orange) buckling modes are shown in Fig. 3, as well. One can utilize the cFSM solutions and superimpose any combinations of pure mode shapes (global mode is mixed) with arbitrary half-wave length along the CFS member as GI. The black dashed line curves in Fig. 3 are similar to the lowest eigenvalues obtained from FE analysis.

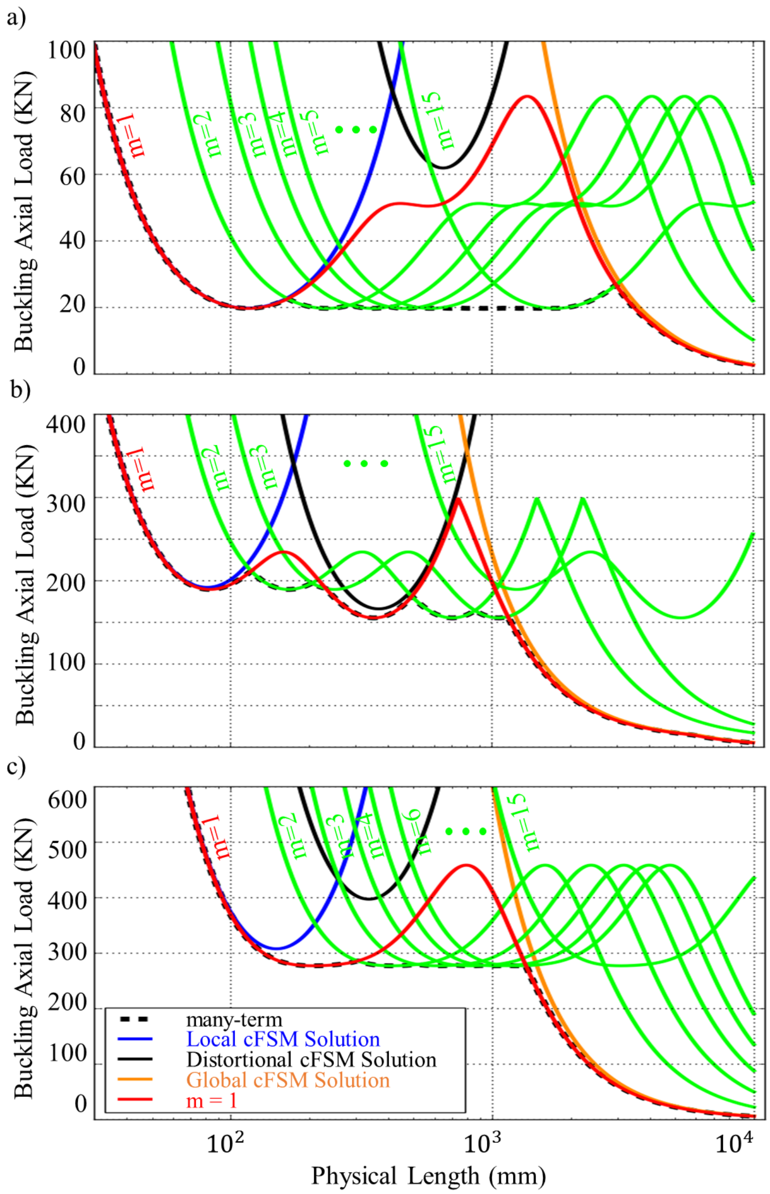

Figure 3: Stability solution of FSM augmented with pure mode cFSM solutions for (a) Case 1 (b) Case 2 (c) Case 3

Fig. 4 shows the modal participation curves for the three cases discussed above. In Fig. 4a, local buckling is the dominant mode of instability for a wide range of lengths (lower than $L{\sim}3000\ mm$) in Case 1. This can also be deduced from Fig. 3a where it is observed that the "many-term" stability solution can be obtained by stitching the first local minima regions of single-term solutions. Similar to Case 1, modal participation curves for Cases 2 and 3 are depicted in Figs. 4b and 4c. It can be seen that Case 2 represents a predominantly distortional buckling behavior at least for a wide range of lengths (the length interval associated with the predominantly red part in Fig. 4b). Case 3, however, is more complicated as the dominant buckling mode is not identifiable. As mentioned before, for CFS members with the same behavior as Case 3 (local-distortional buckling behavior), cFSM has to be used for the purpose of modal identification.

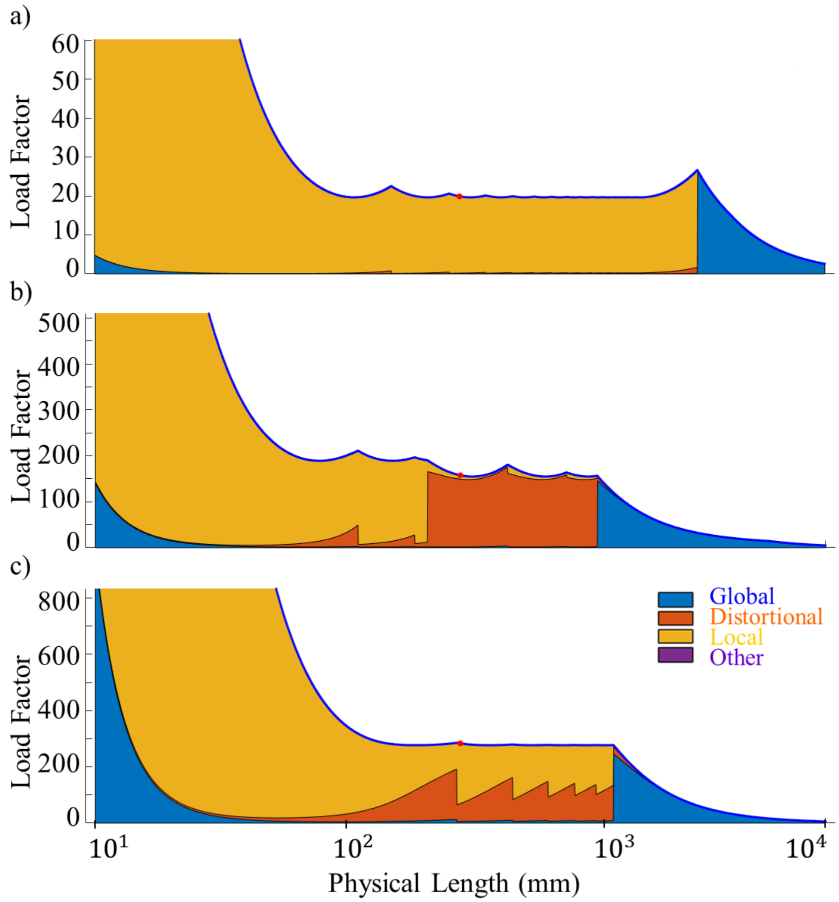

Figure 4: Modal participation for (a) Case 1 (b) Case 2 (c) Case 3

5. Comparative study

Despite significant studies on the influence of GI on LCC of CFS members, the combinatorial role of different GI shapes forming Eq. 1 for a member with an arbitrarily dominant buckling mode has not been fully examined yet. In Section 5.1, we undertake such examination. Further, the responses of models with as-measured imperfections are presented in Section 5.2. Finally, in section 5.3, we provide a brief comparative study of some of the approaches to GI modeling discussed in this paper. By comparison of such multitude GI modeling, we demonstrate the noticeable variability in the load carrying capacity and post-buckling behavior that could stem from adaptation of a wide array of strategies to seeding geometric imperfections into FE analysis models.

5.1 Coupled role of imperfection shape and combination coefficient

The coupled effect of imperfection shape (ϕ_i) and combination coefficient (c_i) on the LCC is investigated by excluding the role of imperfection magnitude (α_i). The cross-section with distortional dominant buckling mode (Case 2) with length $L = 668\ mm$ is considered. The LCC for member without GI equals to 164075 N. Five imperfection magnitudes each corresponding to %80 of LCC for perfect model are identified from the construction of Knock Down Factor (KDF) curves for geometrically imperfect models each involving only one of the modal forms (local, distortional, ...); see Fig. 5.

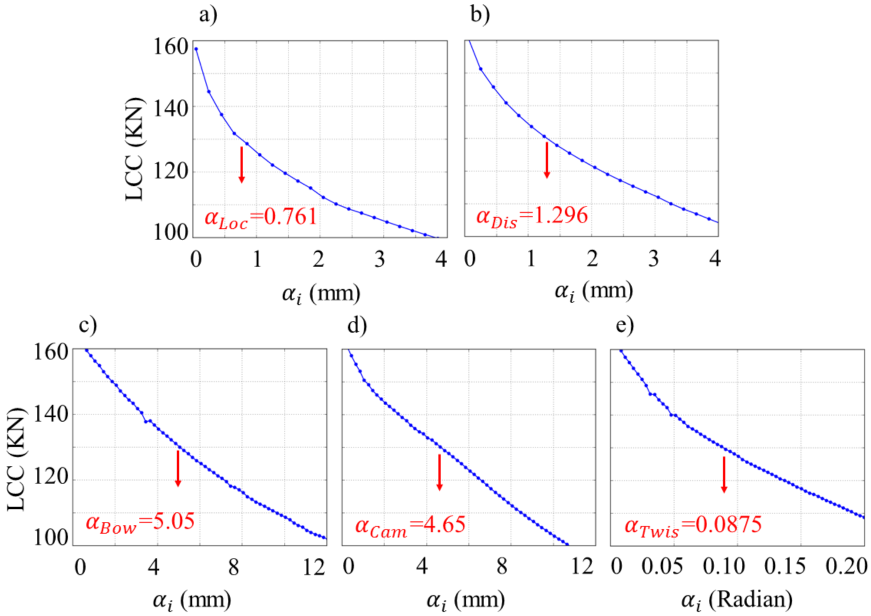

Figure 5: KDF curves and identified imperfection magnitudes corresponding to %80 LCC of perfect model: (a) Local (b) Distortional (c) Bow (d) Camber (e) Twist; Case 2 with $L = 668\ mm$

The force-displacement curves obtained from nonlinear buckling analysis for all combinations of five α_i values and $c_i = -1, 0, 1$ (a total of $3^5 = 243$ combinations) are depicted in Fig. 6. From the inset in Fig. 6, it can be observed that the coupled effect of ϕ_i and c_i results in %37 variation (absolute values vary between 82 to 130 KN) in the load carrying capacity indicating the importance of combination strategy. It can also concluded from these results that GI models affine to only the first buckling mode shape may result in LCC values that are tangibly non-conservative.

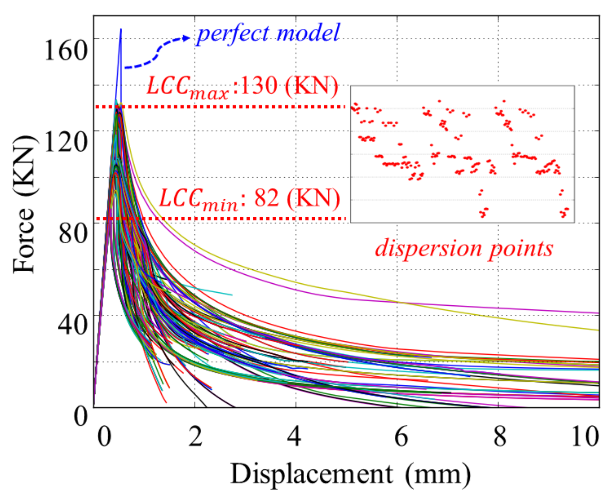

Figure 6: Force-displacement curves for 243 combinatorial GI models of Case 2. The inset represents the dispersion points of LCC

5.2 As-measured geometric imperfection

To provide a general sense about the variability of LCC and stability behavior of of real CFS members, a set of the geometric imperfections as measured in (Peterman 2012) are considered. The samples are 40 studs, all with an identical cross-section (362S162-68) and length (2.438 m).

The numerical results of these imperfect studs with two different boundary conditions are presented in Fig. 7; For details on data processing of measured imperfections and model creations, see (Farzanian et al. 2018b).

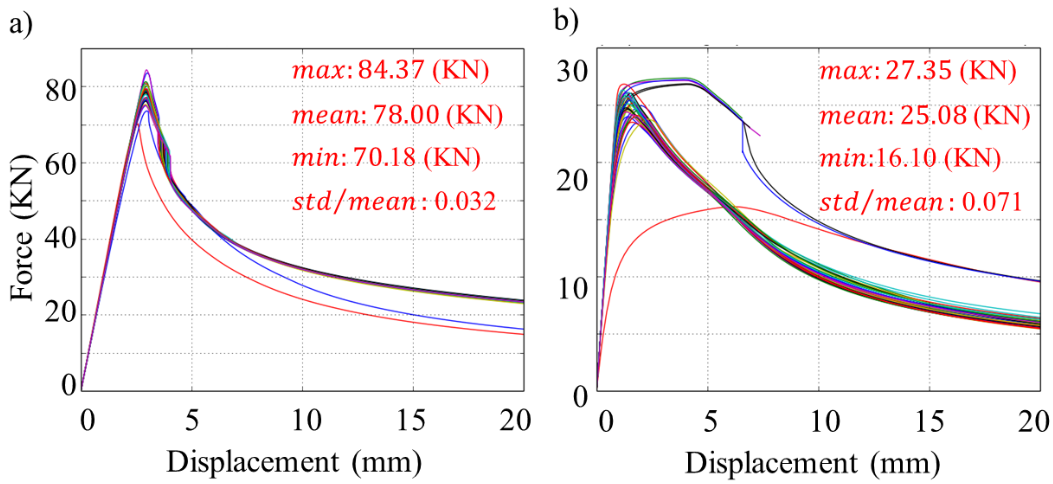

Figure 7: Force-displacement curves for as-measured imperfections with BC of (a) Fixed-Fixed (b) Pinned-Pinned

The minimum, mean, and maximum values of LCC plus its coefficient of variation ares mentioned in the inset of Fig. 7. The results not only show the range of variation in LCC but also the impact of BC on load-displacement responses.

5.3 Geometric imperfections proposed in literature

To investigate the effect of GI model choice, a number of models discussed in Section 2 are considered. Again, the cross-section with distortional dominant buckling mode (Case 2) with length $L = 668\,mm$ is analyzed. The shape of GI's are extracted from either ABAQUS or CUFSM packages. As can be seen from Fig. 8 and Table 2 the choice of GI model has a tangible impact on LCC of CFS member.

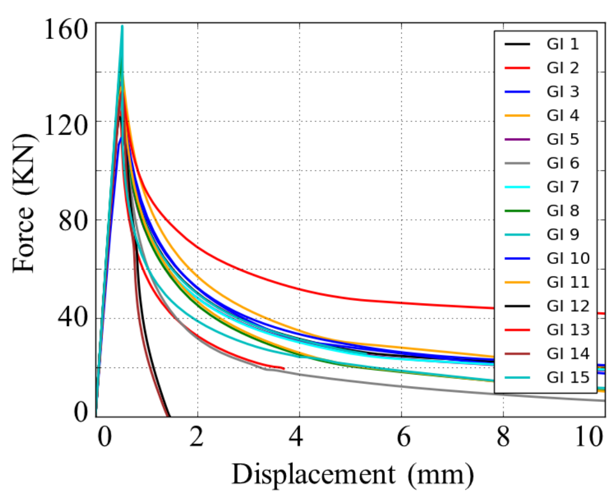

Figure 8: Force-displacement curves for 15 GI models proposed in literature; Case 2

Table 2. Summary of LCC from ABAQUS collapse analysis for different GI models

GI Models	Shape	Magnitude	LCC (KN)
GI 1	Mode[1] 1	$0.333t$	131.89
GI 2	Mode[1] 2	$0.333t$	132.66
GI 3	Mode[1] 3	$0.333t$	133.45
GI 4	Mode[1] 4	$0.333t$	139.49
GI 5	Mode[1] 5	$0.333t$	135.76
GI 6	Modes[1] 1 to 5	$0.333t$	126.53
GI 7	Mode[1] 1	$\gamma(\sigma_y/\sigma_{cr})$	145.64
GI 8	Loc[2]	$\gamma(\sigma_y/\sigma_{cr})$	145.99
GI 9	Mode[1] 1	$d_1 = 0.006w$	132.25
GI 10	Mode[1] 1	$d_2 = t$	113.03
GI 11	Loc[2]	$d_1 = 0.006w$	133.65
GI 12	Dis[2]	$d_2 = t$	121.64
GI 13	Loc+Dis+Bow+Cam+Tws[2]	$50\%ile$	131.82
GI 14	Loc+Dis[2]	$50\%ile$	130.60
GI 15	Bow (half-sine)[2]	L/960	158.59

1. Fundamental mode shapes from ABAQUS
2. Classified mode shapes (Local, Distortional, Bow, Camber, Twist) from CUFSM

6. Conclusions

In this study a brief review on characterizing and modeling of geometric imperfections in numerical simulations of cold-formed steel (CFS) members is performed. A general expression for imperfection profile is presented that can represent all studied imperfection models. The expression is comprised of three ingredients, i.e., imperfection shape, magnitude, and combination coefficient. An automated in-house set of Python and MATLAB scripts coupled with ABAQUS and CUFSM software packages are developed to generate the various imperfect models and are used to report a comprehensive numerical study on load carrying capacity (LCC) and buckling behavior. The studies on the different geometric imperfection modeling strategies reveal the following. For CFS members with a complicated dominant buckling mode, constrained Finite Strip Method or similar tools have to be used for modal identification. The choice of combinations for geometric imperfection shapes results in tangible variation of LCC. Imperfections affine to only a particular buckling mode shape may result in non-conservative prediction of LCC. Choice of boundary condition affects the sensitivity of LCC to imperfections. Predicted variability of LCC based on as-measured imperfection models demonstrates the need for providing probabilistic approaches in design guidelines. This work is part of an ongoing study to enable analysis-based design procedures for CFS members.

Acknowledgments

This work was supported by grants CMMI-1351742, CMMI-1235238 and CMMI-1235196 from National Science Foundation. This support is gratefully acknowledged.

References

Ahmadi, B., Farzanian, S., Asadpoure, A., Schafer, B. W. and Tootkaboni, M. (2018) 'A Chebyshev-Ritz finite strip method for buckling analysis of cold-formed steel members with general boundary conditions', *In Submission.*

BS 5950 (1987) 'British Standards Institution: Part 5 – Structural Use of Steelwork in Buildin: Code of practice for design of cold formed sections'.

Chilver, A. H. (1953) 'The stability and strength of thin-walled steel struts', *The engineer,* 196(5089), 180-183.

Chou, S. M. and Chai, G. B. (1997) 'Ultimate design load of thin–walled stub columns', *International Journal of Computer Applications in Technology,* 10(1-2), 27-33.

Chou, S. M., Chai, G. B. and Ling, L. (2000) 'Finite element technique for design of stub columns', *Thin-Walled Structures,* 37(2), 97-112.

Crisfield, M. (1981) 'A fast incremental/iterative solution procedure that handles "snap-through"', *Computers & Structures,* 13(1-3), 55-62.

Dawson, R. G. and Walker, A. C. (1972) 'Post-buckling of geometrically imperfect plates', *Journal of the Structural Division,* 98(1), 75-94.

Dutheil, J. (1952) 'The theory of instability through disturbance of equilibrium'*, Proceedings of the 4th Congress of IABSE*, translated by Association Internationale des Pont et Charpentes, 275-295.

Farzanian, S., Louhghalam, A., Schafer, B. W. and Tootkaboni, M. (2018a) 'Validation of geometric imperfection models for CFS structural members, Part I: A comparative review of the current models', *In Submission.*

Farzanian, S., Louhghalam, A., Schafer, B. W. and Tootkaboni, M. (2018b) 'Validation of geometric imperfection models for CFS structural members, Part II: Data-driven stochastic modeling and validation metrics', *In Submission.*

Farzanian, S. and Shahsavari, R. (2018) 'Mapping the coupled role of structure and materials in mechanics of platelet-matrix composites', *Journal of the Mechanics and Physics of Solids,* 112, 169-186.

Gardner, L. (2002) 'A new approach to structural stainless steel design', *Ph.D. thesis, Imperial College London.*

Hancock, G. J. (1981) 'Non linear analysis of thin sections in compression', *Journal of the Structural Division*, 25(1), 455-471.

Li, Z. and Schafer, B. W. (2010) 'Buckling analysis of cold-formed steel members with general boundary conditions using CUFSM conventional and constrained finite strip methods', *20th Internaltional Specialised Conference on Cold-Formed Steel Structures*, 17-34.

Peterman, K. D. (2012) 'Experiments on the stability of sheathed cold-formed steel studs under axial load and bending', *Ph.D. thesis, The Johns Hopkins University*.

Peterman, K. D. and Schafer, B. W. (2014) 'Sheathed cold-formed steel studs under axial and lateral load', *Journal of Structural Engineering,* 140(10), 04014074.

Schafer, B. W. and Peköz, T. (1998) 'Computational modeling of cold-formed steel: characterizing geometric imperfections and residual stresses', *Journal of constructional steel research,* 47(3), 193-210.

Schafer, B. W. and Ádány, S. (2006) 'Buckling analysis of cold-formed steel members using CUFSM: conventional and constrained finite strip methods'*, 18th International Specialty Conference on Cold-Formed Steel Structures*, 39-54.

Sivakumaran, K. S. and Abdel-Rahman, N. (1998) 'A finite element analysis model for the behaviour of cold-formed steel members', *Thin-walled structures,* 31(4), 305-324.

NZS 3404 (1997) 'Steel Structures Standards: Part 1', Standards New Zealand, Wellington.

Sun, J. and Butterworth, J. W. (1998) 'Behaviour of steel single angle compression members axially loaded through one leg', *Proceedings of the Australasian Structural Engineering Conference*, 859-866.

Vieira Jr, L. C. M. and Schafer, B. W. (2012) 'Behavior and design of sheathed cold-formed steel stud walls under compression', *Journal of Structural Engineering,* 139(5), 772-786.

Walker, A. C. (1969) 'The post-buckling behaviour of simply-supported square plates', *The Aeronautical Quarterly,* 20(3), 203-222.

Winter, G. (1947) 'Strength of thin steel compression flanges', *Trans. ASCE,* 112, 527.

Zaras, J. and Rhodes, J. (1987) 'Carefully controlled compression tests on thin-walled cold-formed sections', *Applied solid mechanics,* 2, 519-551.

Zeinoddini, V. M. and Schafer, B. W. (2012) 'Simulation of geometric imperfections in cold-formed steel members using spectral representation approach', *Thin-Walled Structures,* 60, 105-117.

Zeinoddini-Meimand, V. (2011) 'Geometric imperfections in cold-formed steel members', *Ph.D. thesis, The Johns Hopkins University*.

Zhao, X., Tootkaboni, M. and Schafer, B. W. (2015) 'Development of a Laser-Based Geometric Imperfection Measurement Platform with Application to Cold-Formed Steel Construction', *Experimental Mechanics,* 55(9), 1779-1790.

Zhao, X., Tootkaboni, M. and Schafer, B. W. (2017) 'Laser-based cross-section measurement of cold-formed steel members: Model reconstruction and application', *Thin-Walled Structures,* 120, 70-80.